1990

The Effects of Separator Design on the Discharge Performance of a Starved Lead-Acid Cell

T. V. Nguyen
Texas A & M University - College Station

Ralph E. White
University of South Carolina - Columbia, white@cec.sc.edu

Hiram Gu

Publication Info

Journal of the Electrochemical Society, 1990, pages 2998-3004.

http://www.electrochem.org/
DOI: 10.1149/1.2086148
http://dx.doi.org/10.1149/1.2086148

The Effects of Separator Design on the Discharge Performance of a Starved Lead-Acid Cell

T. V. Nguyen[1] **and R. E. White***

Department of Chemical Engineering, Texas A&M University, College Station, Texas 77843-3122

Hiram Gu*

Physical Chemistry Department, General Motors Research Laboratories, Warren, Michigan 48090-9055

ABSTRACT

A mathematical model of a starved lead-acid cell has been developed to study the dynamic behavior of the cell during discharge. Concentrated binary electrolyte theory and a volume-averaging technique were used to model the transport of electrolyte. The model can be used to predict cell voltage and profile of: acid concentration, overpotential, porosity, reaction rate, and electrode capacity, as functions of time. The effects of separator thickness and its porosity were examined with respect to cold-cranking amperage and reserve capacity of the battery. The separator was found to be a significant factor governing performance.

Starved lead-acid batteries are becoming increasingly popular in the secondary battery market due to many of their potential advantages: zero maintenance, operation in any position, internal gas pressure potentially usable as a built-in charge indicator, and low battery profile and weight, which is especially attractive in automotive SLI (starting-lighting-ignition) applications. A traditional flooded-type lead-acid battery contains excess acid to compensate for the water loss due to oxygen evolution on overcharge. A unit cell of the battery is composed of a positive electrode, an acid reservoir, a separator, and a negative electrode. A starved lead-acid cell does not have an acid reservoir. Instead, a thicker and more porous separator is used to prevent physical contact of the positive and negative electrodes, serve as an electrolyte reservoir (this gives rise to the concept of an immobilized electrolyte), and promote oxygen gas transport from the positive electrode to the negative electrode for recombination on charging.

The separator has always been thought to play a critical role in the operation of a starved lead-acid battery. Atlung and Fastrup (1), extending the work of Turner and Moseley (2), developed a mathematical model to study the effects of separator design on discharge rate and cell capacity. Their model, however, is of the separator alone, with constant reaction fluxes used as boundary conditions. We present here a detailed mathematical model of the whole starved lead-acid cell for discharge, which will allow the analysis of the total system and interactions between the components—positive electrode, separator, and negative electrode. This model is a modification of an earlier model by Gu *et al.* (3) for the flooded-type cell. With this model, the effects of porosity, tortuosity, thickness, and the level of electrolyte saturation of the separator, on the discharge performance of a starved lead-acid cell, can be studied, including any interactions between the separator and the electrodes.

This paper is organized in the following manner. In the "Model Description" section, detailed formulation of the model is given. In the "Model Output" section, the model results are illustrated graphically using an example of a CCA calculation. Each plot is briefly discussed regarding its significance. In the latter section, the effects due to the separator on cold-cranking amperage (CCA) and reserve capacity (RC) are evaluated in greater detail.

Model Description

A typical starved lead-acid cell is shown schematically in Fig. 1 and consists of the following boundaries and regions: a lead-grid current collector at $x = 0$, which is at the center of the positive (PbO_2) electrode; a positive electrode (region 1); a positive electrode/separator interface; a porous separator (region 2); a separator/negative electrode interface; a negative (Pb) electrode (region 3); and the center of the negative electrode, where another grid is located ($x = l$). The positive and negative electrodes consist of porous solid matrices whose pores are flooded by a binary electrolyte—concentrated H_2SO_4 consisting of H^+ and HSO_4^- in H_2O (4). The model is one-dimensional in the x-direction, perpendicular to the face of the electrode. During discharge, the solid species in a starved lead-acid cell react with H^+ and HSO_4^- as follows

$$PbO_{2(s)} + HSO_4^- + 3H^+ + 2e^- \rightarrow PbSO_{4(s)} + 2H_2O \quad \text{(positive electrode)}$$

and

$$Pb_{(s)} + HSO_4^- \rightarrow PbSO_{4(s)} + 2e^- + H^+ \quad \text{(negative electrode)}$$

For both electrodes, a solid product of $PbSO_4$ is formed on discharge, which changes the porosity and reaction surface area of the electrodes.

The one-dimensional macro-homogeneous model for a starved lead-acid cell presented here consists of the following explicit dependent variables: concentration of the electrolyte c; potential in the solid phase for each electrode ϕ_1; potential in the electrolyte ϕ_2; superficial current density in the electrolyte i_2; and porosity of each porous region ϵ. The independent variables are the spatial coordinate x and time t. The governing equations and boundary conditions for the three regions in the cell are presented next.

Center of the positive electrode.—At this boundary ($x = 0$), the boundary conditions are

$$\frac{\partial c}{\partial x} = 0 \qquad [1]$$

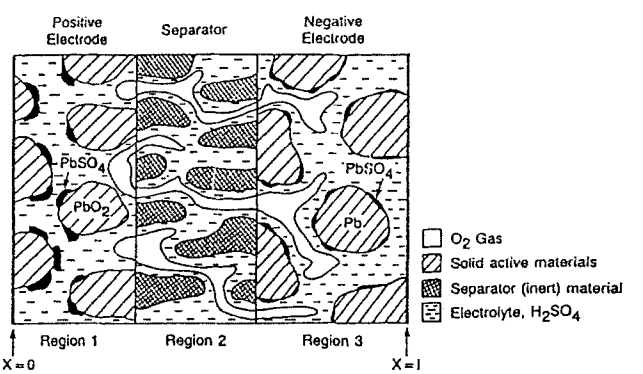

Fig. 1. A one-dimensional macro-homogeneous model for a starved lead-acid cell.

* Electrochemical Society Active Member.
[1] Present address: Los Alamos National Laboratory, Los Alamos, New Mexico 87545

$$i_2 = 0 \quad [2]$$

$$\phi_1 = 0 \quad [3]$$

$$\frac{\partial \phi_2}{\partial x} = 0 \quad [4]$$

The center of the positive electrode consists of a metal current collector sandwiched between two porous electrode matrices. Equations [1] and [4] reflect symmetry at this boundary. Equation [2] states that, at the center of the positive electrode, all the current is in the current collector and none is in the electrolyte. Equation [3] is used to designate ϕ_1 to be a 0 V at this boundary. Without this reference potential, a particular solution cannot be obtained. The fifth equation that we used at this boundary is Eq. [5], as shown for region 1, which describes porosity variations.

Region 1, positive electrode.—

Porosity variation

$$\frac{\partial \epsilon}{\partial t} = \frac{1}{2\mathbf{F}}\left(\frac{\mathrm{MW}_{\mathrm{PbSO_4}}}{\rho_{\mathrm{PbSO_4}}} - \frac{\mathrm{MW}_{\mathrm{PbO_2}}}{\rho_{\mathrm{PbO_2}}}\right)\frac{\partial i_2}{\partial x} \quad [5]$$

Ohm's law in solution

$$\frac{i_2}{\epsilon^{\mathrm{ex1}}\kappa} = -\frac{\partial \phi_2}{\partial x} + \frac{RT}{\mathbf{F}}(1 - 2t^\circ_+)\frac{\partial \ln (cf)}{\partial x} \quad [6]$$

Charge balance

$$i_2 - \epsilon^{\mathrm{exm1}}\sigma_{\mathrm{PbO_2}}\frac{\partial \phi_1}{\partial x} = i_{\mathrm{app}} \quad [7]$$

Material balance

$$\epsilon\frac{\partial c}{\partial t} = D\frac{\partial}{\partial x}\left(\epsilon^{\mathrm{ex1}}\frac{\partial c}{\partial x}\right) + \frac{1}{2\mathbf{F}}\left[-c\left(\frac{\mathrm{MW}_{\mathrm{PbSO_4}}}{\rho_{\mathrm{PbSO_4}}} - \frac{\mathrm{MW}_{\mathrm{PbO_2}}}{\rho_{\mathrm{PbO_2}}}\right) + (3 - 2t^\circ_+)\right]\frac{\partial i_2}{\partial x} \quad [8]$$

Electrode kinetics

$$\frac{\partial i_2}{\partial x} = a_{\mathrm{max1}} i_{\mathrm{o1,ref}}\left(\frac{c}{c_{\mathrm{ref}}}\right)^{\gamma 1}\left(\frac{Q_1}{Q_{\mathrm{max1}}}\right)^{\zeta 1}\left\{\exp\left[\frac{\alpha_{\mathrm{a1}}\mathbf{F}}{RT}(\phi_1 - \phi_2 - \Delta U_{\mathrm{PbO_2}})\right] - \exp\left[\frac{-\alpha_{\mathrm{c1}}\mathbf{F}}{RT}(\phi_1 - \phi_2 - \Delta U_{\mathrm{PbO_2}})\right]\right\} \quad [9]$$

where

$$\Delta U_{\mathrm{PbO_2}} = U_{\mathrm{PbO_2}} - U_{\mathrm{Pb}} \quad [10]$$

Equations [5] describes the change in porosity in region 1 with time due to the conversion of the active solid material by the electrode reaction. Equation [6], a modified Ohm's law for the electrolyte, states that the current in the electrolyte is driven by the electric potential and concentration gradients. Equation [7] is Ohm's law applied to the solid matrix. Equation [8] states that the electrolyte concentration at any point in space changes with time because of electrode reaction, diffusion, and migration. The exponents ex1 and exm1 on the porosity ϵ (cf. Eq. [6] and [7]) are used to account for the geometry of the porous electrode and can be regarded as factors that describe the tortuosity of the porous electrode. Equation [9] has been selected to represent electrode kinetics. The parameters $\gamma 1$, α_{a1}, and α_{c1} are related to the symmetry factor of the rate-determining step of the electrode reaction.

Interface between region 1 and region 2.—

$$\epsilon^{\mathrm{ex1}}\left.\frac{\partial c}{\partial x}\right|_{\text{region 1}} = (f_{\mathrm{sat}}\epsilon_{\mathrm{sep}})^{\mathrm{ex2}}\left.\frac{\partial c}{\partial x}\right|_{\text{region 2}} \quad [11]$$

$$\frac{\partial \epsilon}{\partial t} = \frac{1}{2\mathbf{F}}\left(\frac{\mathrm{MW}_{\mathrm{PbSO_4}}}{\rho_{\mathrm{PbSO_4}}} - \frac{\mathrm{MW}_{\mathrm{PbO_2}}}{\rho_{\mathrm{PbO_2}}}\right)\left.\frac{\partial i_2}{\partial x}\right|_{\text{region 1}} \quad [12]$$

$$i_2 = i_{\mathrm{app}} \quad [13]$$

$$\left.\frac{\partial \phi_1}{\partial x}\right|_{\text{region 1}} = 0 \quad [14]$$

$$\epsilon^{\mathrm{ex1}}\left.\frac{\partial \phi_2}{\partial x}\right|_{\text{region 1}} = (f_{\mathrm{sat}}\epsilon_{\mathrm{sep}})^{\mathrm{ex2}}\left.\frac{\partial \phi_2}{\partial x}\right|_{\text{region 2}} \quad [15]$$

Equations [11] and [15] satisfy the requirement that the flux of the electrolyte, N_e, and the superficial current density, i_2, are continuous across the interface. In other words, $N_{\mathrm{e,region\,1}} = N_{\mathrm{e,region\,2}}$ and $i_{\mathrm{2,region\,1}} = i_{\mathrm{2,region\,2}}$. The constant f_{sat} is used to specify the fraction of the separator that is filled with electrolyte—not occupied by oxygen. Equation [12] describes the variation of the porosity with time. Equation [13] indicates that all the current at this interface is in the electrolyte phase. Finally, Eq. [14] states that the electrode solid-phase potential gradient is equal to zero at the interface because there is no current in the solid phase at this point (*i.e.*, all of the current is in the electrolyte phase).

Region 2, separator.—

Porosity

$$\epsilon = f_{\mathrm{sat}}\epsilon_{\mathrm{sep}} \quad [16]$$

Ohm's law in solution

$$\frac{i_2}{\epsilon^{\mathrm{ex2}}\kappa} = -\frac{\partial \phi_2}{\partial x} + \frac{RT}{\mathbf{F}}[(1 - 2t^\circ_+)]\frac{\partial \ln (cf)}{\partial x} \quad [17]$$

Solid-phase potential

$$\phi_1 = 0 \quad [18]$$

Material balance

$$\epsilon\frac{\partial c}{\partial t} = D\epsilon^{\mathrm{ex2}}\frac{\partial^2 c}{\partial x^2} \quad [19]$$

Current in solution

$$i_2 = i_{\mathrm{app}} \quad [20]$$

Equation [16] indicates that the effective porosity of the separator available to current flow is fixed by f_{sat}. Equation [17] is Ohm's law applied to the electrolyte. The potential of the electrode solid phase, ϕ_1, is treated in this region as a dummy variable and is set arbitrarily equal to zero (Eq. [18]). Equation [19] is a material balance on the electrolyte in the separator. Finally, Eq. [20] states that all the applied current flows through the solution phase, because we assume that no conductive solid phase exists in the separator.

Interface between region 2 and region 3.—

$$(f_{\mathrm{sat}}\epsilon_{\mathrm{sep}})^{\mathrm{ex2}}\left.\frac{\partial c}{\partial x}\right|_{\text{region 2}} = \epsilon^{\mathrm{ex3}}\left.\frac{\partial c}{\partial x}\right|_{\text{region 3}} \quad [21]$$

$$\frac{\partial \epsilon}{\partial t} = -\frac{1}{2\mathbf{F}}\left(\frac{\mathrm{MW}_{\mathrm{PbSO_4}}}{\rho_{\mathrm{PbSO_4}}} - \frac{\mathrm{MW}_{\mathrm{Pb}}}{\rho_{\mathrm{Pb}}}\right)\left.\frac{\partial i_2}{\partial x}\right|_{\text{region 3}} \quad [22]$$

$$i_2 = i_{\mathrm{app}} \quad [23]$$

$$\left.\frac{\partial \phi_1}{\partial x}\right|_{\text{region 3}} = 0 \quad [24]$$

$$(f_{sat}\epsilon_{sep})^{ex2}\left.\frac{\partial\phi_2}{\partial x}\right|_{region\ 2} = \epsilon^{ex3}\left.\frac{\partial\phi_2}{\partial x}\right|_{region\ 3} \quad [25]$$

The equations for this interface are established with the same reasoning used at the interface between region 1 and region 2.

Region 3, negative electrode.—

Porosity variation

$$\frac{\partial\epsilon}{\partial t} = -\frac{1}{2\mathbf{F}}\left(\frac{MW_{PbSO_4}}{\rho_{PbSO_4}} - \frac{MW_{Pb}}{\rho_{Pb}}\right)\frac{\partial i_2}{\partial x} \quad [26]$$

Ohm's law in solution

$$\frac{i_2}{\epsilon^{ex3}\kappa} = -\frac{\partial\phi_2}{\partial x} + \frac{RT}{\mathbf{F}}(1 - 2t^\circ_+)\frac{\partial \ln (cf)}{\partial x} \quad [27]$$

Charge balance

$$i_2 - \epsilon^{exm3}\sigma_{Pb}\frac{\partial\phi_1}{\partial x} = i_{app} \quad [28]$$

Material balance

$$\epsilon\frac{\partial c}{\partial t} = D\frac{\partial}{\partial x}\left(\epsilon^{ex3}\frac{\partial c}{\partial x}\right) + \frac{1}{2\mathbf{F}}\left[c\left(\frac{MW_{PbSO_4}}{\rho_{PbSO_4}} - \frac{MW_{Pb}}{\rho_{Pb}}\right) + (1 - 2t^\circ_+)\right]\frac{\partial i_2}{\partial x} \quad [29]$$

Electrode kinetics

$$\frac{\partial i_2}{\partial x} = a_{max3}i_{o3,ref}\left(\frac{c}{c_{ref}}\right)^{\gamma 3}\left(\frac{Q_3}{Q_{max3}}\right)^{\zeta 3}\left\{\exp\left[\frac{\alpha_{a3}\mathbf{F}}{RT}(\phi_1 - \phi_2 - \Delta U_{Pb})\right] - \exp\left[\frac{-\alpha_{c3}\mathbf{F}}{RT}(\phi_1 - \phi_2 - \Delta U_{Pb})\right]\right\} \quad [30]$$

Equations [26] through [30] are counterparts of the equations used for the positive electrode (region 1). ΔU_{Pb} is defined as $U_{Pb} - U_{Pb}$ (cf. Eq. [10]), which is zero. It is explicitly expressed to show the similarity between Eq. [30] and Eq. [9].

Center of the negative electrode.—At this boundary ($x = l$), like the other boundary at $x = 0$, the conditions are

$$\frac{\partial c}{\partial x} = 0 \quad [31]$$

$$i_2 = 0 \quad [32]$$

$$\frac{\partial\phi_2}{\partial x} = 0 \quad [33]$$

Since the solid-phase potential was set to zero at $x = 0$, the kinetic expression (Eq. [30]) is used at this boundary to calculate the solid-phase potential, ϕ_1. Equation [26] makes up the fifth equation to be used here.

Numerical procedure.—The model equations were put into finite difference form and solved using implicit stepping and a numerical procedure referred to as pentadiagonal BAND (J) (5). The Crank-Nicolson method was used for the time increment. The model converges with discretization error $O[(\Delta t)^2 + \Delta x)^2]$ (6).

Concentration-dependent parameters.—The diffusion coefficient, D, and conductivity, κ, of the acid are calculated according to the empirical expressions of Tiedemann and Newman (7)

$$D = (1.75 + 260c)10^{-5}\exp\left(7.29 - \frac{2174}{T}\right) \quad [34]$$

$$\kappa = c\left[\exp\left(1.1104 + 199.475c - 1{,}6097.781c^2 + \frac{3{,}916.95 - 9{,}9406c - 72{,}1860/T}{T}\right)\right] \quad [35]$$

One notices that temperature dependency is also included in these equations.

The equilibrium potential ΔU_{PbO_2} (at 25°C) is calculated from an empirical equation (4)

$$\Delta U_{PbO_2} = 1.9228 + 0.147519\log m + 0.063552\log^2 m + 0.073772\log^3 m + 0.033612\log^4 m \quad [36]$$

where m is the molality of the sulfuric acid. Another empirical equation based on literature data at 25°C (4) is used to relate c to m

$$m = 1.00322 \times 10^3 c + 3.55 \times 10^4 c^2 + 2.17 \times 10^6 c^3 + 2.06 \times 10^8 c^4 \quad [37]$$

Although D, κ, and ΔU_{PbO_2} are dependent on c, they are not formulated explicitly in terms of c in the model. In other words, for each spatial node point, they are calculated based on the concentration determined in the previous time step.

Model Output

The model calculates the cell voltage, battery voltage, and five profiles: acid concentration, electrode polarization, electrode porosity, reaction rate, and state-of-charge. The battery voltage is calculated based on six cells connected in series

$$V_{battery}(t) = 6V_{cell}(t) + I_{battery}\left(5R_{ic} + 2R_t + \frac{12R_{grid}}{N_{plate} - 1}\right) \quad [38]$$

where R_{ic} and R_t are measured resistance of the intercell connector and battery terminal, respectively; N_{plate} is the

Table I. Parameters used in the base-line calculation

—Electrolyte—	
Acid concentration (c_{ref})	= 4.9×10^{-3} mol/cm^3 (1.280 sp gr)
Transference number (t°_+)	= 0.72 (7)
—Positive electrode—	
Half thickness of plate	= 0.08 cm
Theoretical capacity (Q_{max1})	= 2620 C/cm^3
Volume fraction of inert filler	= 0.05
Maximum specific surface area (a_{max1})	= 2.3×10^5 cm^2/cm^3
Exchange current density ($i_{o1,ref}$)	= 3.19×10^{-8} A/cm^2 at −18°C = 3.19×10^{-7} A/cm^2 at 25°C
α_{a1}, α_{c1}	= 1.15, 0.85
$\gamma 1$, $\zeta 1$	= 0.3, 1.5
Lead dioxide conductivity (σ_{PbO_2})	= 500 S/cm (4)
ex1, exm1	= 1.5, 0.5
—Separator—	
Thickness of separator	= 0.10 cm
Porosity (ϵ_{sep})	= 0.96
ex2	= 1.50
f_{sat}	= 0.95
—Negative electrode—	
Half thickness of plate	= 0.09 cm
Theoretical capacity (Q_{max3})	= 3120 C/cm^3
Volume fraction of inert filler	= 0.10
Maximum specific surface area (a_{max3})	= 2.3×10^4 cm^2/cm^3
Exchange current density ($i_{o3,ref}$)	= 4.96×10^{-7} A/cm^2 at −18°C = 4.96×10^{-6} A/cm^2 at 25°C
α_{a3}, α_{c3}	= 1.55, 0.45
$\gamma 3$, $\zeta 3$	= 1.0×10^{-4}, 1.5
Lead conductivity (σ_{Pb})	= 48,000 S/cm (4)
ex3, exm3	= 1.5, 0.5

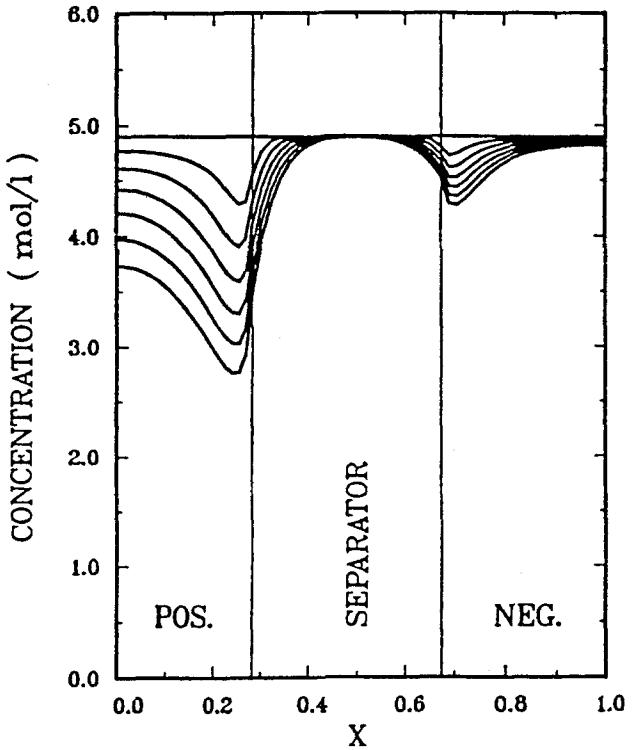

Fig. 2. Electrolyte concentration profiles for 408 mA/cm² discharge at −18°C. Profiles from top to bottom are at time steps of 0, 5, 10, 15, 20, and 30s, respectively.

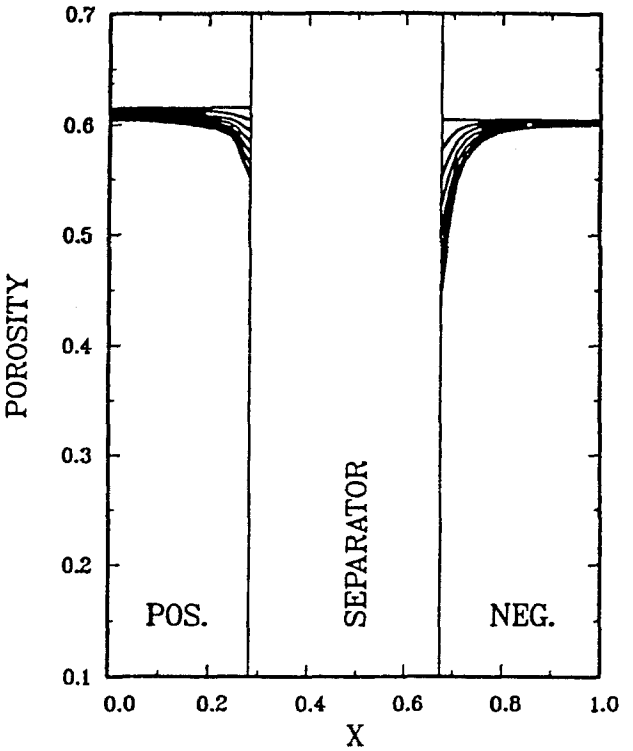

Fig. 4. Electrode porosity profiles for 408 mA/cm² discharge at −18°C. Profiles from top to bottom are at time steps of 0, 5, 10, 15, 20, and 30s, respectively.

total number of plates in each cell; $I_{battery}$ is the discharge current in amperes and has a negative value; $V_{cell}(t)$ is $(\phi_{1,x=0} - \phi_{1,x=l})$; and R_{grid} is the equivalent grid resistance due to both the positive and negative grids. The value of R_{grid} requires an educated estimate based on experimental battery test data and results of a mathematical model of the grid geometry (8).

The results of a simulation—a high-current cold-cranking test of 728A at −18°C on a battery with thirteen 13.9-cm by 10.7-cm plates in each cell—will be illustrated next. The resistances used to calculate the battery voltage are

$$R_{grid} = 1.85 \times 10^{-3} \text{ ohm},$$
$$R_{ic} = 1.00 \times 10^{-4} \text{ ohm}, \quad \text{and}$$
$$R_t = 1.00 \times 10^{-4} \text{ ohm}$$

Other values used for the calculation can be found in Table I.

The development of the electrolyte concentration profile with time (Fig. 2) provides us with information on the

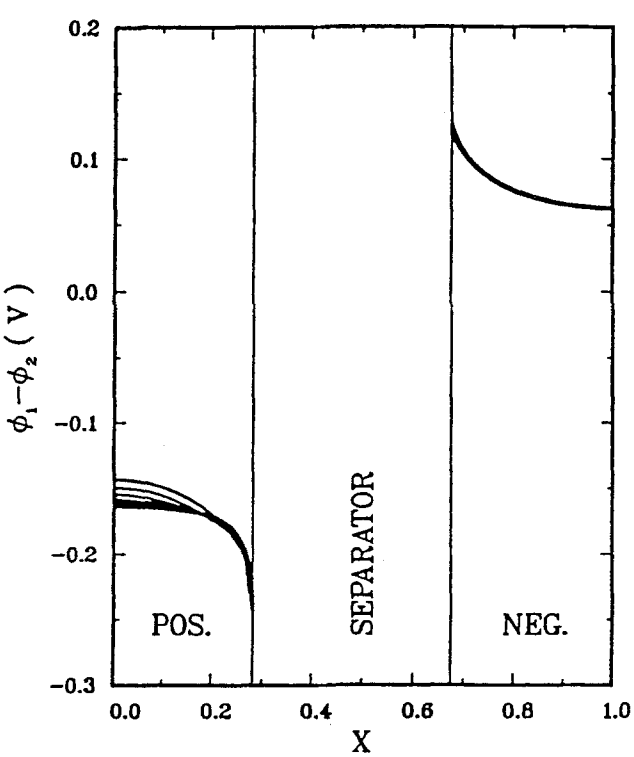

Fig. 3. Electrode polarization profiles for 408 mA/cm² discharge at −18°C.

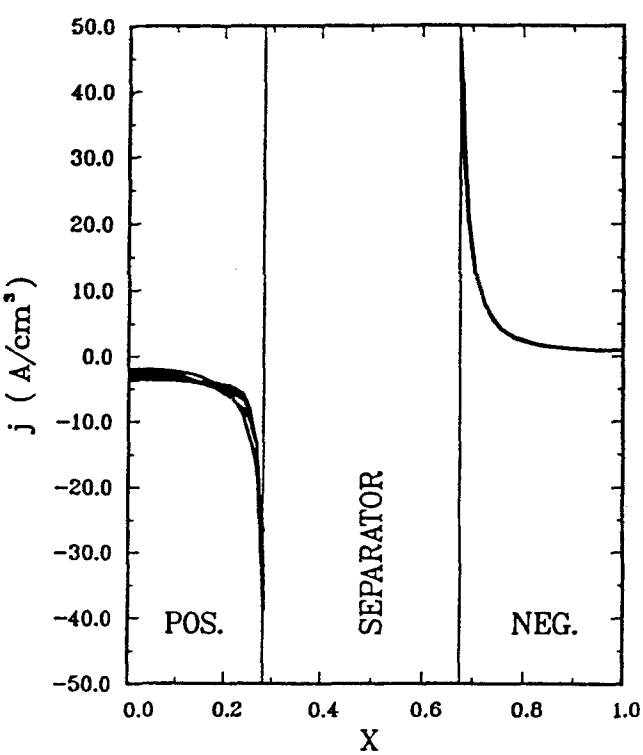

Fig. 5. Reaction rate profiles for 408 mA/cm² discharge at −18°C

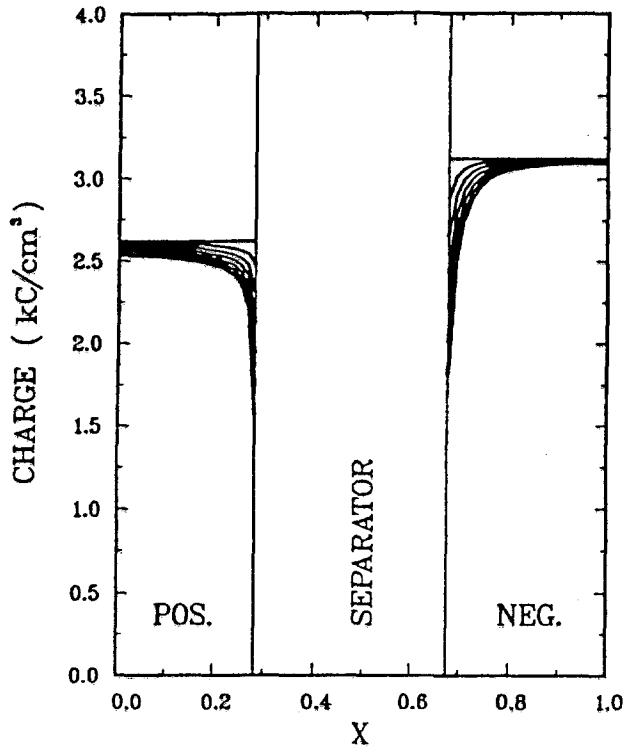

Fig. 6. State-of-charge profiles for 408 mA/cm² discharge at −18°C. Profiles from top to bottom are at time steps of 0, 5, 10, 15, 20, and 30s, respectively.

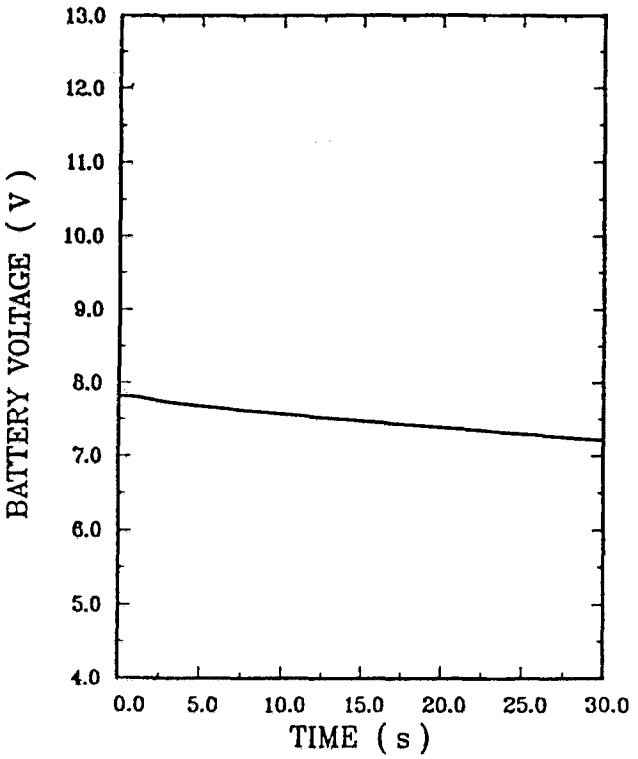

Fig. 8. Battery voltage as a function of time for 408 mA/cm² discharge at −18°C.

availability of the acid for the electrode reaction (especially in the positive electrode). The profile indicates whether acid depletion is limiting the capacity of the cell. For the present case, acid depletion is definitely not a limiting factor. Cold cranking performance of a lead-acid battery is mostly affected by high electrolyte resistivity and slow electrode kinetics (cf. Fig. 7). One sees from Fig. 2 that acid depletion is more noticeable in the positive electrode.

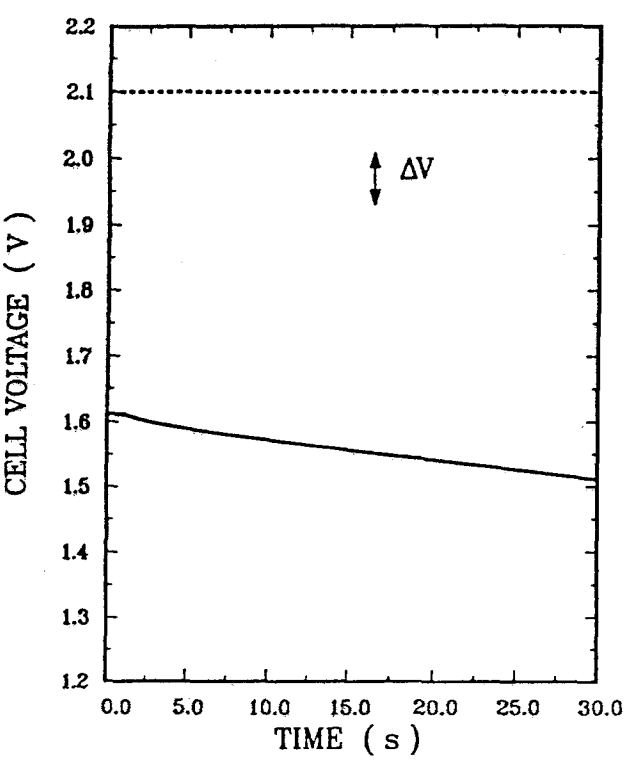

Fig. 7. Cell voltage as a function of time for 408 mA/cm² discharge at −18°C.

The degree of polarization across the thickness of an electrode is the $\phi_1 - \phi_2$ profile. For the present case, Fig. 3 indicates that the polarization of the negative electrode is relatively unchanged during the 30s of discharge. The positive electrode in the beginning of the discharge exhibits a lower polarization near the current collector and a higher polarization at the electrode/separator interface. Toward the end of the discharge, the degree of polarization becomes more uniform across. The acid concentration may play a role in the difference between the positive and negative electrode polarization profiles (cf. Fig. 2).

The porosity profile indicates whether the pores of the electrodes are being plugged by the discharge product—$PbSO_4$. Figure 4 reveals that the negative electrode loses its porosity faster than the positive electrode. The fast drop in porosity at the front of the negative electrode is due to the high reaction rate there (cf. Fig. 5). The reaction rate profile tells us whether the electrode is being utilized uniformly. Figure 5 shows that under the cold cranking conditions both electrodes are nonuniformly discharged. The negative electrode has less uniform reaction distribution—showing a higher rate of reaction at the front of the electrode—as compared to the positive electrode. The reaction rate profile of the positive electrode, however, varies more with time, which is consistent with the polarization profile.

The state-of-charge profile (Fig. 6) is obtained from the time integral of the reaction rate. It shows the cumulative effect of the non-uniform electrode reaction rate. Under cold cranking conditions, the capacity of an electrode is not a limiting factor. The cell voltage (Fig. 7) is a global response to the ohmic losses, concentration polarization, and electrode kinetics. The initial large drop from the open-circuit voltage (~2.1V) indicates that the ohmic and kinetic effects are quite significant at low-temperature cranking. The open-circuit voltage of the battery is six times the open-circuit voltage of a cell. At 30s into the discharge, the battery voltage has dropped to 7.2V (Fig. 8)—the standard cutoff voltage for a cold cranking test. A comparison between the battery and cell voltages gives us an idea of the significance of losses due to the grids, intercell connectors, and terminals.

Effects of the separator.—We used the model to examine the effects of glass-mat separator thickness and glass-mat porosity on the CCA and RC performance of a starved

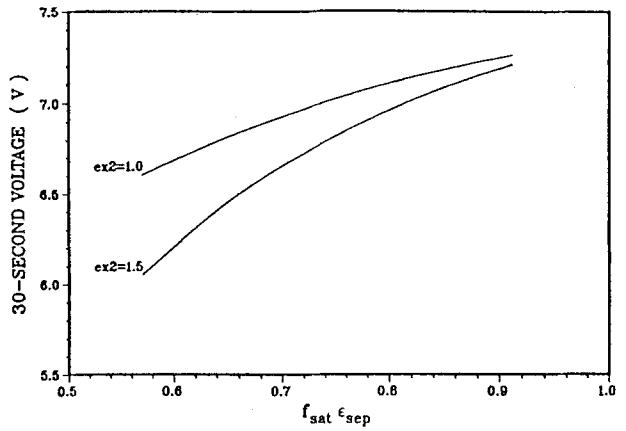

Fig. 9. Effects of separator porosity and saturation level on 30s cranking voltage.

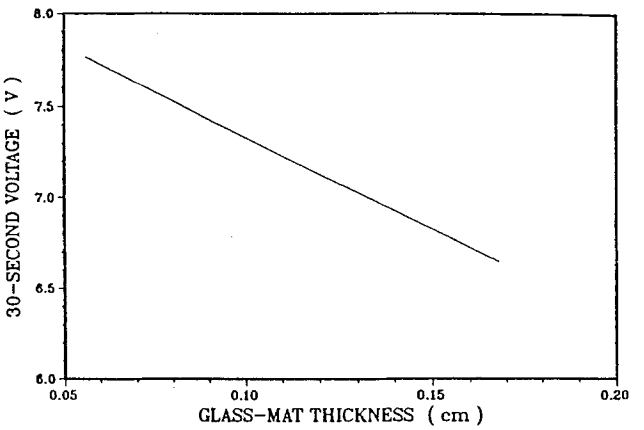

Fig. 11. Effect of separator thickness on 30s cranking voltage

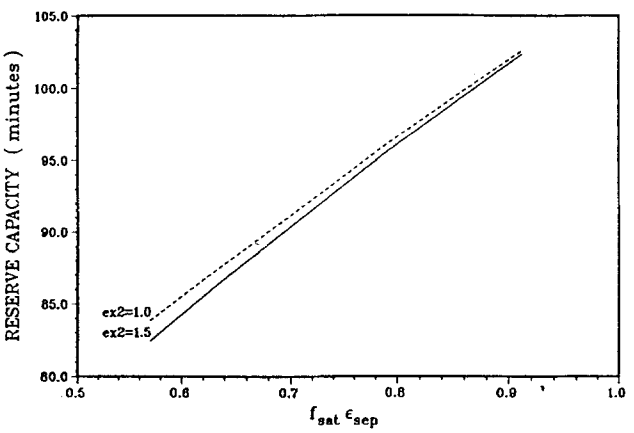

Fig. 10. Effects of separator porosity and saturation level on reserve capacity.

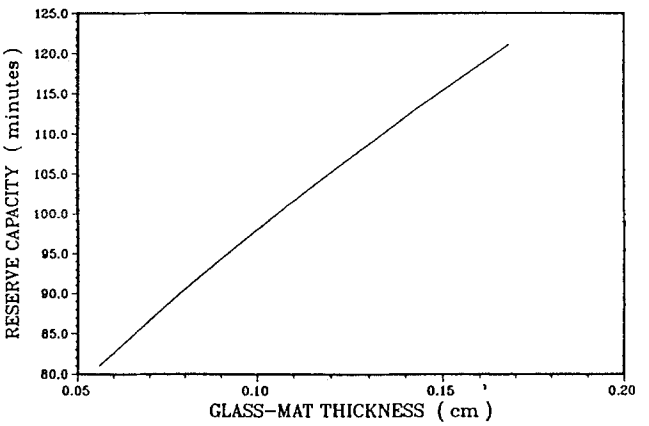

Fig. 12. Effect of separator thickness on reserve capacity

lead-acid battery. The CCA calculation was based on a 728A discharge at −18°C to 30s, as was used to illustrate the results of a model calculation in the last section. The RC calculation was based on a 25A discharge at 25°C to 10.5V of the battery terminal voltage.

In Fig. 9, the 30s voltage is plotted against $f_{sat}\epsilon_{sep}$ at the two tortuosity factors, ex2 of 1.0 and 1.5. All other parameters used are those given in Table I. The abscissa was so chosen because the 30s voltage is really directly affected by the product of f_{sat} and ϵ_{sep}. For instance, the effect is the same whether $\epsilon_{sep} = 0.70$ and $f_{sat} = 0.95$ or $\epsilon_{sep} = 0.96$ and $f_{sat} = 0.69$. From Fig. 9, we see that the effect of the separator porosity on the 30s voltage is not a linear function; one might incorrectly assume, without a detailed analysis, that the voltage drop would be inversely proportional to the cross-sectional area. We also see that the effect of ex2 varies with the porosity level of the separator. The precise knowledge of the tortuosity factor is not as important in predicting 30s voltage when the separator is relatively porous.

The effect of the separator porosity on RC is almost linear, as shown in Fig. 10, indicating that RC is proportional to the volume of electrolyte stored in the separator. This finding suggests that the electrolyte in the separator is sufficiently utilized at the low current discharge and that the diffusion of acid is not limiting. Figure 10 also indicates that an exact knowledge of the tortuosity factor is not important to obtaining a satisfactory prediction of the reserve capacity.

To examine the effects of the separator thickness, we used a porosity of 0.96, a tortuosity factor of 1.5, and all other values of the base-line condition given in Table I. The effects of the separator thickness were found to be quite straightforward. The separator thickness affects the 30s voltage linearly (Fig. 11), as would be expected, since the voltage loss across a conductor is a direct function of the length. The effect of the separator on RC is also approximately linear (Fig. 12) because like the porosity the thickness governs the amount of acid that is available for the electrode reaction—the thicker the separator, the more acid, the greater the reserve capacity.

Conclusions

The separator in a starved lead-acid battery is an important factor governing the performance of the battery. Its thickness and porosity have significant effects on the CCA capability and RC. We can use this mathematical model to select a separator that will give an optimum balance between CCA capability and RC performance. We have also examined the sensitivity of CCA and RC to the tortuosity factor of the separator formulated in the mathematical model. We found that the accuracy of the model in predicting RC is not sensitive to the tortuosity factor, and neither is the CCA prediction if the porosity of the separator is high.

Acknowledgment

The authors acknowledge the support of the Delco-Remy Division of General Motors. We also wish to thank Dr. John S. Dunning of General Motors Research Laboratories for his helpful suggestions.

Manuscript submitted Jan. 29, 1990.

Texas A&M University assisted in meeting the publication costs of this article.

LIST OF SYMBOLS

a_{max1}, a_{max3}	maximum specific active surface area in regions 1 and 3, cm^2/cm^3
c	concentration of the binary electrolyte, mol/cm^3
c_{ref}	reference concentration of the binary electrolyte, mol/cm^3

D	diffusion coefficient of the binary electrolyte, cm^2/s
ex1, exm1	exponents on porosity in region 1
ex2	exponent on porosity in region 2, separator tortuosity factor
ex3, exm3	exponents on porosity in region 3
f	mean molar activity coefficient
f_{sat}	fraction of separator saturated with acid
$\mathbf{F}$	Faraday's constant, 96,487 C/mol
i_{app}	total applied current density based on projected electrode area, A/cm^2
$i_{o1,ref}$	exchange current density at c_{ref} for the positive electrode, A/cm^2
$i_{o3,ref}$	exchange current density at c_{ref} for the negative electrode, A/cm^2
i_2	superficial current density in the solution based on projected electrode area, A/cm^2
$I_{battery}$	applied current, A
j	reaction current per unit volume of electrode, A/cm^3
l	distance between positive and negative electrode current collectors, cm
m	molality of the acid, mol/kg
MW_i	molecular weight of species i (i = $PbSO_4$, PbO_2, Pb), g/mol
n	number of electrons involved in electrode reaction
N_e	flux of electrolyte, mol/cm^2-s
Q_1, Q_3	charge per unit volume in regions 1 and 3, C/cm^3
Q_{max1}, Q_{max3}	maximum charge per unit volume in regions 1 and 3, C/cm^3
N_{plate}	number of plates in a cell
R	universal gas constant, 8.3143 J/mol-K
R_{grid}	equivalent resistance of a pair of positive and negative grids, Ω
R_{ic}	resistance of a battery intercell connector, Ω
R_t	battery terminal resistance, Ω
t	time, s
t°_+	transference number of H^+ with respect to the solvent velocity
T	absolute temperature, K
U_{Pb}, U_{PbO_2}	standard electrode potentials referred to the hydrogen electrode, V
ΔU_{PbO_2}	rest-potential difference between PbO_2 and Pb electrodes, V
$V_{cell}(t)$	cell voltage, V
x	distance from the center of the positive electrode, cm
X	ratio of x to the total cell thickness (with half electrodes)

Greek letters

α_{a1}, α_{c1}	anodic and cathodic transfer coefficients for the positive electrode
α_{a3}, α_{c3}	anodic and cathodic transfer coefficients for the negative electrode
$\gamma 1$, $\gamma 3$	exponents for the concentration dependence of the exchange current density
ϵ	porosity
ϵ_{sep}	porosity of the separator
$\zeta 1$, $\zeta 3$	exponents for the charge dependence of the specific active surface area
κ	electrolyte conductivity, S/cm
ρ_i	density of species i (i = $PbSO_4$, PbO_2, Pb), g/cm^3
σ_i	conductivity of the electrode solid phase (i = Pb, PbO_2), S/cm
ϕ_1	potential in the electrode matrix, V
ϕ_2	potential in the solution, V

Subscripts

e	electrolyte
o	solvent
+	cation
−	anion

REFERENCES

1. S. Atlung and B. Fastrup, *J. Power Sources*, **13,** 39 (1984).
2. A. D. Turner and P. T. Moseley, *ibid.*, **9,** 19 (1983).
3. H. Gu, T. V. Nguyen, and R. E. White, *This Journal*, **134,** 2953 (1987).
4. H. Bode, "Lead Acid Batteries," John Wiley & Sons, New York (1977).
5. J. Van Zee, G. Kleine, R. E. White, and J. Newman, "Electrochemical Cell Design," R. E. White, Editor, Plenum Press, New York (1984).
6. B. Carnahan, H. A. Luther, and J. O. Wilkes, "Applied Numerical Methods," John Wiley & Sons, Inc., New York (1969).
7. W. H. Tiedemann and J. Newman, in "Battery Design and Optimization," (PV 79-1) S. Gross, Editor, p. 23, The Electrochemical Society Softbound Proceedings Series, Princeton, NJ (1979).
8. H. Gu, *This Journal*, **130,** 1459 (1982).

Topotactic Two-Phase Reaction of Ruthenium Dioxide (Rutile) in Lithium Nonaqueous Cell

Tsutomu Ohzuku,* Keijiro Sawai, and Taketsugu Hirai*

Electrochemistry and Inorganic Chemistry Laboratory, Department of Applied Chemistry, Faculty of Engineering, Osaka City University, Sugimoto 3-3-138, Sumiyoshi, Osaka 558, Japan

ABSTRACT

Electrochemical and x-ray diffraction studies were carried out for the reduction of RuO_2 having rutile structure in 1*M* $LiClO_4$ propylene carbonate/1,2-dimethoxyethane (1:1) solution. RuO_2 was topotactically reduced to $LiRuO_2$, drawing an L-shaped voltage curve. X-ray diffraction examinations of the reduced RuO_2 indicated that RuO_2 (tetragonal; a = 4.491Å, c = 3.105Å) was transformed to $LiRuO_2$ (orthorhombic; a = 5.055Å, b = 4.954Å, c = 2.774Å) via an intermediate phase having a tetragonal lattice (a = 4.65Å, c = 3.10Å). The reaction was reversible, *i.e.*, $LiRuO_2$ was electrochemically oxidized to RuO_2 via an intermediate phase. Although three phases coexisted during the reduction of RuO_2 and oxidation of $Li_{1.0}RuO_2$, the reaction was classified as a topotactic two-phase reaction in which an intermediate phase existed between the RuO_2 and $LiRuO_2$ phases. Hysteresis was observed, even in plots of the open-circuit voltages (OCV) *vs.* the reduction degree, when the cell was cycled. The reaction mechanism of RuO_2 is discussed, with emphasis on one characteristic of a topotactic two-phase reaction. The mechanochemical aspects on the reaction are also described.

Insertion electrodes are of great interest among battery researchers and electrochemists because of their utility as cathode materials for lithium nonaqueous cells. Of these, manganese dioxide (MnO_2) has attracted interest since its applicability to rechargeable lithium cells was indicated (1-4). In order to develop the electrochemistry of MnO_2 in a lithium nonaqueous cell, it is necessary to understand the electrochemistry of rutile (2).

Heat-treated electrolytic manganese dioxide (HEMD) at 400°C is widely used as a cathode material for primary lith-

* Electrochemical Society Active Member.